iScience

CellPress
OPEN ACCESS

Article

Schwann cells-derived exosomal miR-21 participates in high glucose regulation of neurite outgrowth

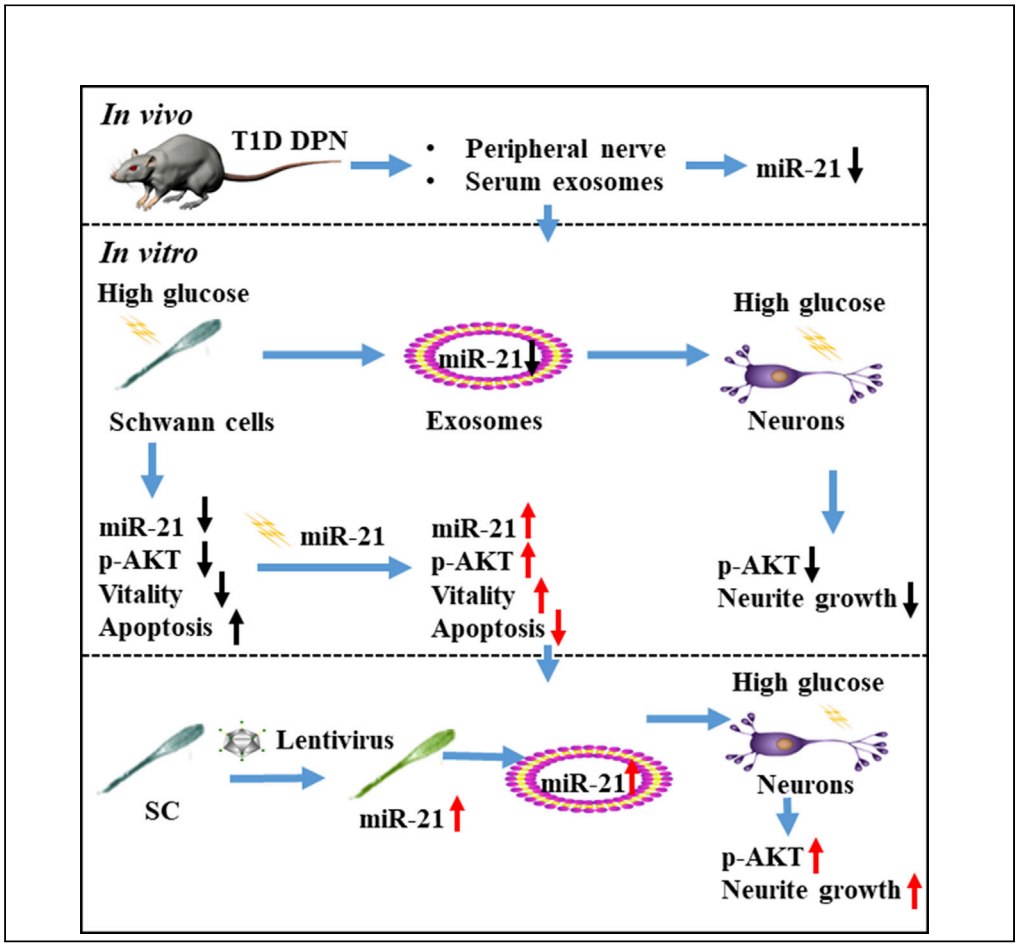

Yu-pu Liu, Ming-yue Tian, Yi-duo Yang, ..., Guo-hong Cui, Hai-dong Guo, Shui-jin Shao

gh_cui@qq.com (G.-h.C.)
hdguo8@hotmail.com (H.-d.G.)
shaoshuijin@163.com (S.-j.S.)

Highlights

The miR-21 was decreased in serum exosomes and sciatic nerve of DPN rats

High glucose inhibited SC viability and downregulated the expression of miR-21

Exosomes derived from SC cultured in high glucose inhibited the neurite outgrowth

SC-derived exosomes rich in miR-21 accelerated the neurite outgrowth of neuron

Liu et al., iScience 25, 105141
October 21, 2022
https://doi.org/10.1016/j.isci.2022.105141

iScience

CellPress
OPEN ACCESS

Article

Schwann cells-derived exosomal miR-21 participates in high glucose regulation of neurite outgrowth

Yu-pu Liu,[1,2,5] Ming-yue Tian,[1,5] Yi-duo Yang,[1] Han Li,[1] Tian-tian Zhao,[1] Jing Zhu,[1] Fang-fang Mou,[1] Guo-hong Cui,[3,*] Hai-dong Guo,[1,4,*] and Shui-jin Shao[1,6,*]

SUMMARY

As a common complication of diabetes, the pathogenesis of diabetic peripheral neuropathy (DPN) is closely related to high glucose but has not been clarified. Exosomes can mediate crosstalk between Schwann cells (SC) and neurons in the peripheral nerve. Herein, we found that miR-21 in serum exosomes from DPN rats was decreased. SC proliferation was inhibited, cell apoptosis was increased, and the expression of miR-21 in cells and exosomes was downregulated when cultured in high glucose. Increasing miR-21 expression reversed these changes, while knockdown of miR-21 led to the opposite results. When co-cultured with exosomes derived from SC exposed to high glucose, neurite outgrowth was inhibited. On the contrary, neurite outgrowth was accelerated when incubated with exosomes rich in miR-21. We further demonstrated that the SC-derived exosomal miR-21 participates in neurite outgrowth probably through the AKT signaling pathway. Thus, SC-derived exosomal miR-21 contributes to high glucose regulation of neurite outgrowth.

INTRODUCTION

Approximately 20% of type I diabetic (T1D) and 50% of type II diabetic (T2D) patients are affected by diabetic peripheral neuropathy (DPN) (Hicks and Selvin, 2019). DPN usually manifests as a feeling of pain and numbness. DPN not only has a tremendous impact on patient's quality of life but also affects the mortality rate (approximately 25%–50% within 5–10 years). The pathogenesis of DPN has not yet been fully elucidated; however, hyperglycemia is viewed as a major factor that plays an important role in the development of DPN (Levitt et al., 1996).

MicroRNAs (miRNAs) are small RNA with a length of 18–28 nucleotides (Jagadeeswaran et al., 2012), which can mediate gene silencing. They are involved in almost all biological processes (O'Brien et al., 2018), and their importance in the field of peripheral nerve injury (PNI) and regeneration has been widely recognized (Sullivan et al., 2018). MiR-21 was upregulated after PNI (Karl et al., 2017; Sakai and Suzuki, 2013, Yu et al., 2011). Upregulation of miR-21 plays an important role in promoting Schwann cells (SC) proliferation, cell apoptosis of adult dorsal root ganglion neurons, and axon regeneration (Luo et al., 2017; Zhou et al., 2015; Ning et al., 2020). Interestingly, reduced miR-21 levels were found in the peripheral nerve and circulation of T2D model mice (Wang et al., 2020a; Wu et al., 2020).

SC form a myelin sheath to protect axons (Salzer, 2015) and there is a close metabolic interaction between SC and axons (Bouçanova and Chrast, 2020). Exosomes are extracellular vesicles secreted by cells and are in a size range of 40–160 nm (Kalluri and LeBleu, 2020). As miRNA carriers (Yu et al., 2016), SC-derived exosomes can be specifically internalized by axons and enhance regeneration after PNI (Lopez Verrilli et al., 2013). Additionally, exosomes can also reverse the reduction in miR-21 levels induced by diabetes, promote neurite outgrowth, and improve sciatic nerve conduction velocity (NCV) in DPN mice (Wang et al., 2020a).

Here, we explored whether miR-21 levels were reduced in the peripheral nerve and circulation of T1D DPN model rats, then we focused on whether SC-derived exosomal miR-21 participates in high glucose regulation in NG108-15 cells (simulation of peripheral neurons (Ching et al., 2018)) neurite outgrowth, to provide a

[1]Department of Anatomy, School of Basic Medicine, Shanghai University of Traditional Chinese Medicine, Shanghai 201203, China

[2]Department of Orthopaedics, Shanghai Key Laboratory for Prevention and Treatment of Bone and Joint Diseases, Shanghai Institute of Traumatology and Orthopaedics, Ruijin Hospital, Shanghai Jiao Tong University School of Medicine, Shanghai 200025, PR China

[3]Department of Neurology, Shanghai No. 9 People's Hospital, Shanghai Jiaotong University School of Medicine, Shanghai 200011, China

[4]Academy of Integrative Medicine, Shanghai University of Traditional Chinese Medicine, Shanghai 201203, China

[5]These authors contributed equally

[6]Lead contact

*Correspondence: gh_cui@qq.com (G.-h.C.), hdguo8@hotmail.com (H.-d.G.), shaoshuijin@163.com (S.-j.S.)

https://doi.org/10.1016/j.isci.2022.105141

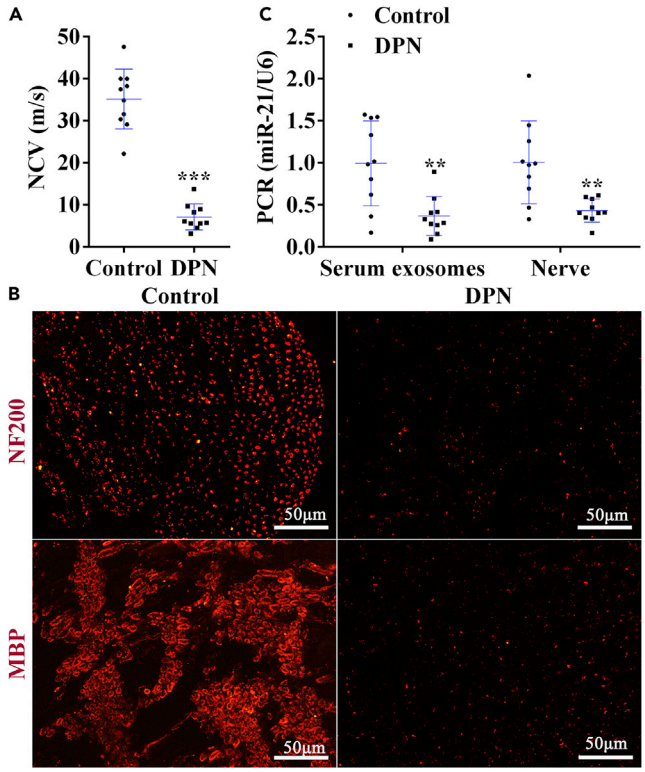

Figure 1. The expression of miR-21 in serum exosomes and sciatic nerve was downregulated

(A) The NCV of DPN rats was significantly lower than that of the control group (n = 10 rats).

(B) Immunocytochemistry staining of NF200 (red) and MBP (red) reflected the morphology of axons and myelin. The number of axons and myelin was significantly reduced in DPN rats compared with the control group. Scale bar: 50 μm. The expression of miR-21 in serum exosomes and sciatic nerve was detected by qPCR (n = 10 rats).

(C) The level of miR-21 was decreased in serum exosomes and sciatic nerve of DPN rats (n = 10 rats). For the above, data are represented as mean ± SD (t-test: $^{**}p < 0.01$, $^{***}p < 0.001$ versus the control group).

reasonable basis for the application of SC-derived exosomal miR-21 for investigating the mechanisms and treatment of DPN.

RESULTS

The expression of miR-21 was decreased in serum exosomes and sciatic nerve of DPN rats

To investigate the expression changes of miR-21 in serum exosomes and peripheral nerves of DPN rats, we first established the T1D DPN model and found that the NCV of DPN rats was significantly lower than that of the control group (Figure 1A). In addition, the number of axons and myelin was significantly reduced in DPN rats compared with the control group, and the shape of myelin was changed (Figure 1B). These results demonstrated that the DPN model was successfully established. The expression of miR-21 in serum exosomes and sciatic nerve was detected by PCR, and we found that the level of miR-21 was decreased in serum exosomes and sciatic nerve of DPN rats (Figure 1C).

High glucose inhibited SC proliferation, increased cell apoptosis, and downregulated the expression of miR-21 in cells and exosomes

We then explored the impact of a high-glucose environment on SC and the changes of miR-21 *in vitro*. Cell viability varies regularly with glucose concentration (Figures S1A and S1B), and therefore 3 typical concentrations were chosen. Effects of high glucose on SC were detected after treatment with low glucose (1 g/L), normal glucose (4.5 g/L), or high glucose (18 g/L) by performing a CCK-8 cell viability assay. The results showed that cell proliferation of SC has been inhibited in the high glucose group compared with the low and normal glucose group at 48 h and 72 h; the low glucose group had the best cell viability. In future

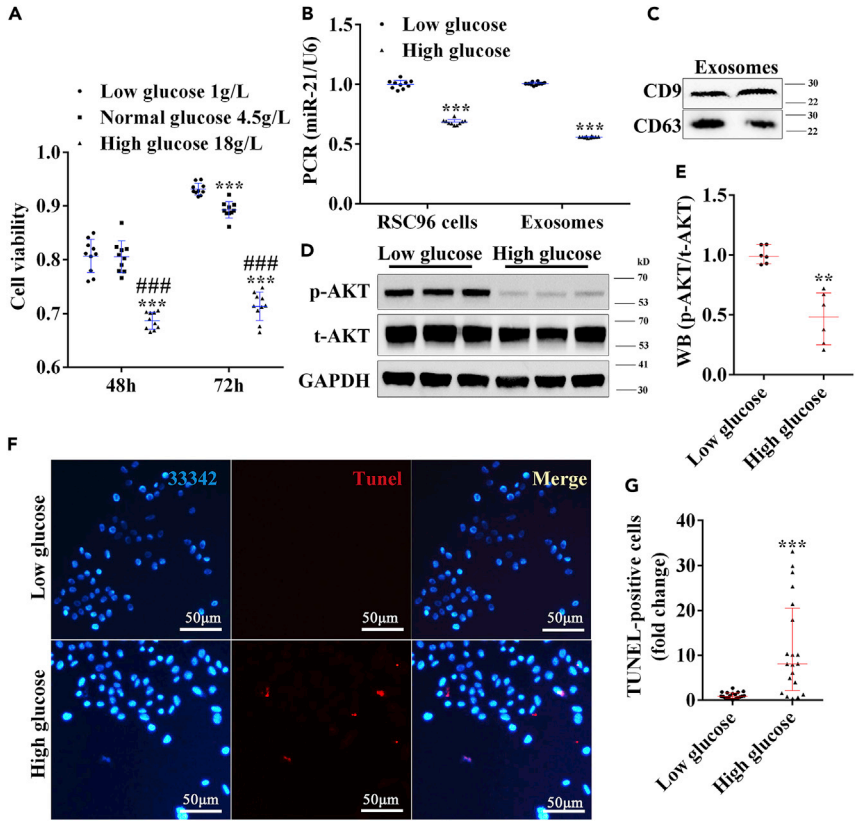

Figure 2. High glucose conditions inhibited SC proliferation, increased cell apoptosis, and downregulated the expression of miR-21 in cells and exosomes

(A) The cell viability of SC was examined by CCK-8 assay, high glucose causes cell viability to decrease (n = 10-well, one-way ANOVA: ***p < 0.001 versus the low glucose group. $^{###}$p < 0.001 versus the normal glucose group).

(B) The expression of miR-21 in SC and exosomes was detected by qPCR, and miR-21 was downregulated in the high glucose group compared with that of the low glucose group (n = 10 samples; t-test: ***p < 0.001 versus the low glucose group).

(C) Exosome markers (CD9 and CD63) were detected by Western blot after exosomes were isolated by ultracentrifugation.

(D and E) Protein expression of *p*-AKT, t-AKT, and GAPDH was detected by Western blot (D), and the expression of the AKT signaling pathway was decreased in the high glucose group compared with that of the low glucose group. (E) Gray value statistics of Western blot (n = 6 samples, nonparametric tests (Mann-Whitney Test, same below): **p < 0.01 versus the low glucose group).

(F and G) TUNEL assay (F) was used to detect cell apoptosis (red), apoptosis increased in the high glucose group compared with the low glucose group. Scale bar: 50 μm.

(G) Cell apoptosis statistics (n = 20 fields of view per group, nonparametric tests: ***p < 0.001 versus the low glucose group). For the above, data are represented as mean ± SD.

experiments, the normal glucose group was excluded, and 72 h was used as the time-point since the differences between the groups were obvious at 72 h (Figure 2A).

Exosomes were isolated by ultracentrifugation and were characterized by exosome markers (CD9 and CD63) detected with Western blot (Figure 2C). After RNA purification from SC and exosomes, miR-21 expression was detected by qPCR. Expression of miR-21 in cells and exosomes was downregulated in the high glucose group compared with the low glucose group (Figure 2B). Detection of protein expression of *p*-AKT, t-AKT, and GAPDH by Western blot indicated that the expression of proteins associated with the AKT signaling pathway was significantly decreased under high glucose conditions in SC (Figures 2D and 2E). We used the TUNEL assay to identify and quantify apoptotic cells and observed increased cell apoptosis of SC in the high glucose group (Figures 2F and 2G). The above results indicate that miR-21 may play an important role in the pathogenesis of DPN.

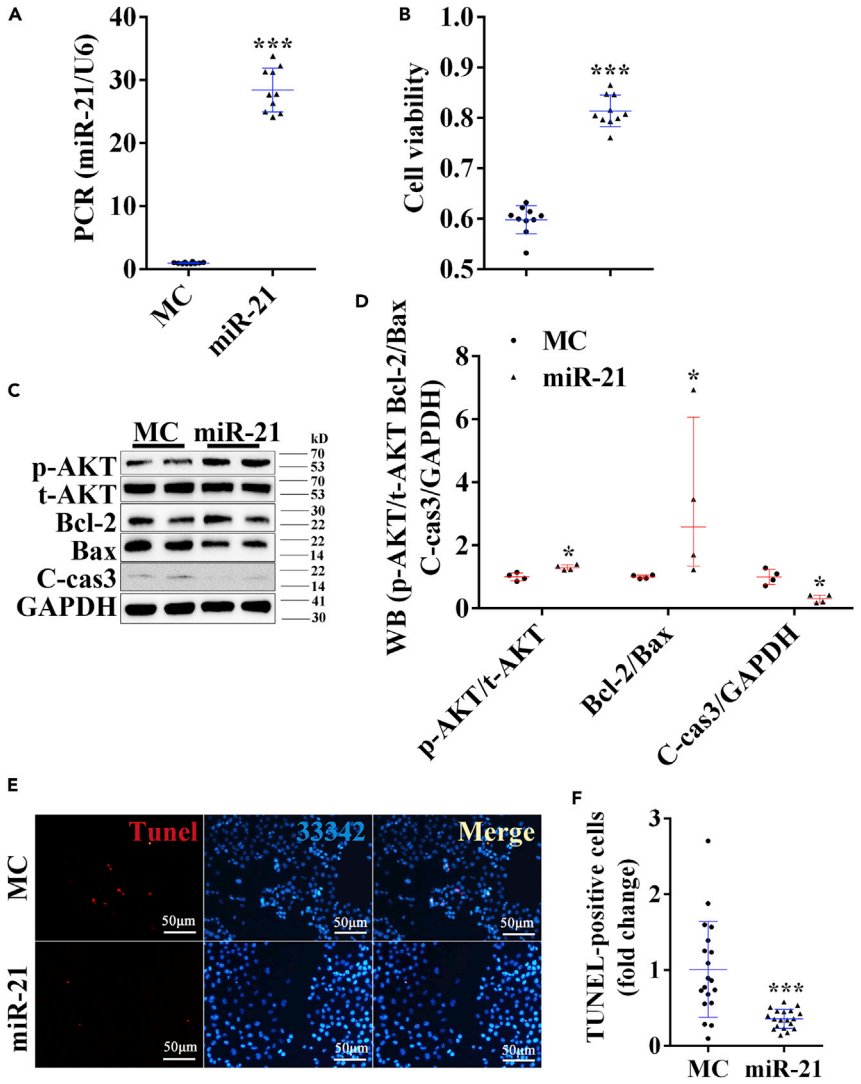

Figure 3. Upregulation of miR-21 enabled SC viability and reduced cell apoptosis in high glucose conditions

(A) miR-21 expression in SC were detected by PCR, and miR-21 expression was upregulated after transfection of miR-21 mimic compared with the MC group (n = 10 samples, t-test: ***p < 0.001 versus the MC group).

(B) The cell viability of SC was examined by CCK-8 assay and upregulation of miR-21 resulted in a significant increase in SC viability compared with the MC group (n = 10-well; t-test: p < 0.001 versus the MC group).

(C and D) Protein expression of *p*-AKT, t-AKT, Bcl-2, Bax, C-cas3, and GAPDH in SC was detected by Western blot (C), results showed that compared with the MC group, the upregulation of miR-21 resulted in increased expression of Bcl-2/Bax, while decreased expression of C-cas3/GAPDH. (D) Gray value statistics of Western blot (n = 4 samples, nonparametric tests: *p < 0.05 of *p*-AKT/AKT, Bcl2/Bax and C-cas3/GAPDH versus the MC group).

(E and F) TUNEL assay (E) to detect SC cell apoptosis (red) showed that increasing miR-21 levels reduced cell apoptosis in SC under high glucose conditions compared with the MC group. Scale bar: 50 μm. (F) Cell apoptosis statistics (n = 20 fields of view per group, t-test: ***p < 0.001 versus the MC group). For the above, data are represented as mean ± SD.

Increasing levels of miR-21 enabled SC viability and reduced cell apoptosis in high glucose conditions

To clarify the regulatory role of miR-21 in DPN *in vitro*, we next explored the effects of miR-21 on SC in high glucose. We performed a qRT-PCR assay to verify that miR-21 expression was upregulated after transfection of the miR-21 mimic (Figure 3A). The upregulation of miR-21 led to a significant increase in SC viability compared with the mimic control (MC) group (Figure 3B). The AKT signaling pathway was activated, as shown by Western blot (Figures 3C and 3D). We also determined Bcl-2/Bax and Cleaved Caspase-3 (C-cas3/GAPDH) protein expression because these proteins are related to the regulation of cell apoptosis;

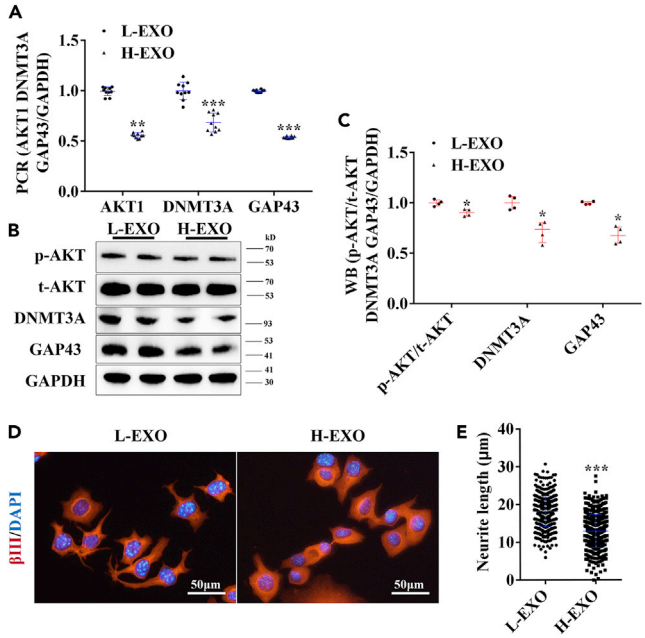

Figure 4. High glucose-induced SC-derived exosomes inhibited the neurite outgrowth of NG108-15 cells in high glucose

(A) Expression of AKT1, DNMT3A, and GAP43 in NG108-15 was detected by PCR, and AKT signaling pathway and neurite outgrowth-related factors (DNMT3A and GAP43) were inhibited in NG108-15 cells treated with H-EXO compared to L-EXO (n = 10 samples; t-test: ***p < 0.001 versus the L-EXO group).

(B and C) Western blot (B) was used to detect the protein expression of *p*-AKT, t-AKT, DNMT3A, and GAP43 in NG108-15 cells, the results had the same trend as the PCR results. (C) Gray value statistics of Western blot (n = 4 samples, nonparametric tests: *p < 0.05 of *p*-AKT/AKT, Bcl2/Bax and C-cas3/GAPDH versus the L-EXO group).

(D and E) Immunocytochemistry staining (D) of beta III Tubulin (red) to observe neurite outgrowth, H-EXO significantly reduced neurite outgrowth in NG108-15 cells compared to L-EXO. Scale bar: 25 μm. (E) Neurite length quantification (n = 10 fields of view per group, t-test: ***p < 0.001 versus the L-EXO group). For the above, data are represented as mean ± SD.

a TUNEL assay was also performed. The results showed that upregulation of miR-21 causes an increase in the expression of Bcl-2/Bax and a concomitant decrease in the expression of C-cas3/GAPDH (Figures 3C and 3D), suggesting that under high glucose conditions, increasing levels of miR-21 reduced cell apoptosis of SC. The TUNEL assay results also confirmed these findings (Figures 3E and 3F).

SC-derived exosomes induced by high glucose levels inhibited the neurite outgrowth of NG108-15 cells

Degeneration of distal axons of peripheral neurons progresses in DPN, and exosomes can exchange materials and information between SC and peripheral neurons and their axons. To detect the effect of exosomes secreted by SC on neuronal cell lines under high glucose, exosomes (L-EXO and H-EXO) were extracted from the cell culture supernatants of SC cultured in low glucose or high glucose for 72 h. NG108-15 cells exposed to high glucose conditions were added with L-EXO or H-EXO daily for 3 days. Then, total RNA and protein were isolated from the cells. PCR and Western blot were used to detect the AKT signaling pathway and neurite growth-related factors (DNMT3A, and GAP43), respectively. The results demonstrated that the AKT signaling pathway and neurite growth-related factors were suppressed in NG108-15 cells treated with H-EXO compared with L-EXO (Figures 4A–4C). Immunocytochemistry staining of βIII was used to stain the cytoskeleton, thus we could observe and measure the length of the neurites. We discovered that H-EXO significantly decreased neurite outgrowth of NG108-15 cells (12.99 ± 4.373 μm vs. 18.17 ± 4.110 μm in the L-EXO group; Figures 4D and 4E). It shows that exosomes secreted by SC under a high-glucose environment can inhibit the growth of neuronal processes, and as mentioned in the previous results, the expression of miR-21 in exosomes has changed, suggesting miR-21 may be an important regulatory factor in exosomes.

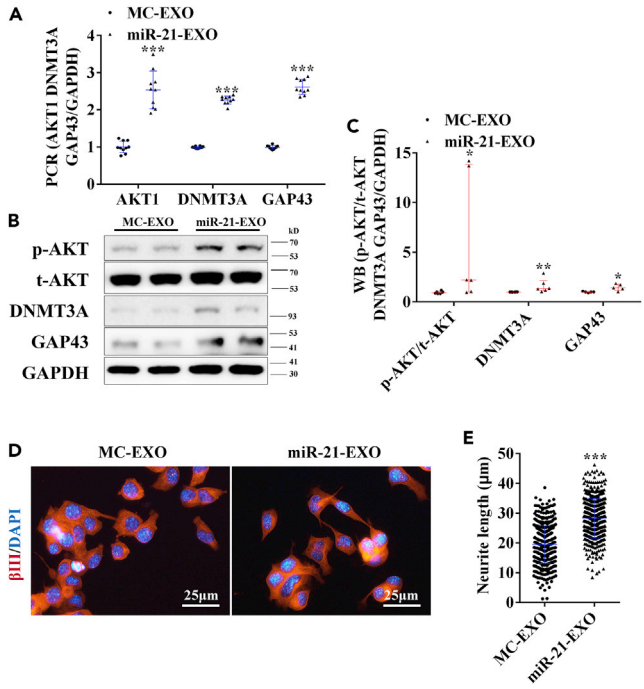

Figure 5. SC-derived exosomes rich in miR-21 accelerated the neurite outgrowth of NG108-15 cells under high glucose conditions

(A) Expression of AKT1, DNMT3A, and GAP43 in NG108-15 was detected by PCR, and AKT signaling pathway and neurite outgrowth-related factors (DNMT3A, GAP43) were enhanced in NG108-15 cells treated with miR-21-EXO compared to MC-EXO (n = 10 samples, t-test: ***p < 0.001 versus the MC-EXO group).

(B and C) Western blot (B) was used to detect the protein expression of *p*-AKT, t-AKT, DNMT3A, and GAP43 in NG108-15 cells, the results had the same trend as the PCR results. (C) Gray value statistics of Western blot (n = 6 samples, nonparametric tests: *p < 0.05 of *p*-AKT/AKT/GAP43/GAPDH, **p < 0.01 of DNMT3A/GAPDH versus the MC-EXO group).

(D and E) Immunocytochemistry staining (D) of beta III Tubulin (red) to observe neurite outgrowth. Scale bar: 25 μm. (E) Neurite length quantification (n = 10 fields of view per group, t-test: ***p < 0.001 versus the MC-EXO group). For the above, data are represented as mean ± SD.

SC-derived exosomes rich in miR-21 accelerated the neurite outgrowth of NG108-15 cells in high glucose conditions

Finally, we explored the effect of altering the expression of miR-21 in exosomes secreted by SC on neuronal cell lines. Two stable SC cell lines transfected using lentiviral vectors expressing empty or the precursor of miR-21-5p, respectively, were constructed. These 2 SC cell lines were cultured in DMEM with 10% exosome-free FBS for 72 h, and exosomes (MC-EXO and miR-21-EXO) were extracted from the cell culture supernatant. NG108-15 cells exposed to high glucose conditions were added with MC-EXO or miR-21-EXO for 3 days, and then total RNA and protein were isolated from the cells. Interestingly, the AKT signaling pathway and neurite growth-related factors were elevated in NG108-15 cells treated with miR-21-EXO compared with MC-EXO, as detected by PCR and Western blot (Figures 5A–5C). Immunocytochemistry staining of βIII to measure the length of neurite confirmed that miR-21-EXO stimulated neurite outgrowth of NG108-15 cells (28.36 ± 6.629 μm v's 19.49 ± 6.289 μm in MC-EXO group; $p < 0.01$; Figures 5D and 5E), indicating that SC-derived exosomal miR-21 participates in high glucose regulation of neurite outgrowth.

MiR-21 knockdown in SC inhibited cell proliferation and increased cell apoptosis

Furthermore, we also explored the effect of miR-21 knockdown in SC to further clarify the role of miR-21 in DPN. SC were transfected with miR-21 NC control or its inhibitor for 48 h. We performed an RT-qPCR assay to verify the expression of miR-21 was downregulated after transfection of the miR-21 inhibitor (Figure 6A). SC proliferation was significantly inhibited after the downregulating of miR-21 compared with the NC control group (Figure 6B). A TUNEL assay showed that downregulation of miR-21 significantly promoted SC apoptosis (Figures 6C and 6D).

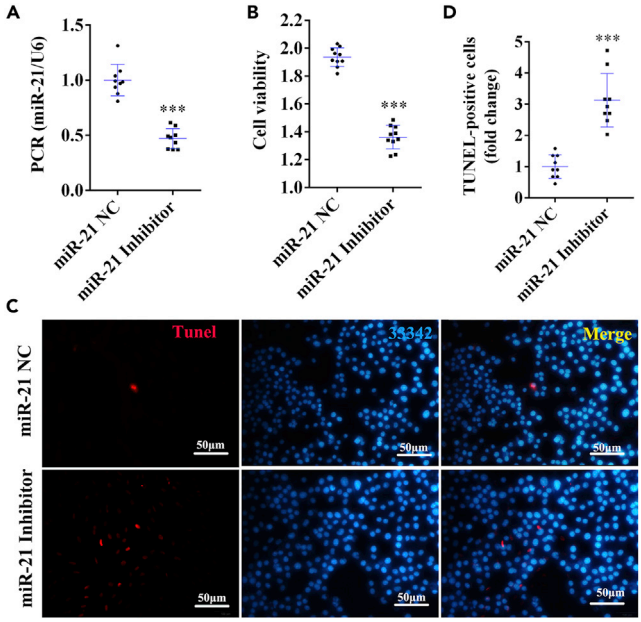

Figure 6. MiR-21 Knockdown in SC inhibited cell proliferation and increased cell apoptosis

(A) miR-21 expression in SC was detected by PCR, and miR-21 expression was downregulated after transfection of miR-21 inhibitor compared with the NC group (n = 10 well).

(B) The cell viability of SC was examined by CCK-8 assay and downregulation of miR-21 resulted in a significant reduction in SC viability compared with the NC group.

(C and D) TUNEL assay (C) showed that knockdown of miR-21 increased cell apoptosis in SC compared with the NC group. Scale bar: 50 μm. (D) Cell apoptosis statistics. (n = 10 fields of view per group, t-test: ***$p < 0.001$ versus the NC control group). For the above, data are represented as mean ± SD.

DISCUSSION

Some diabetic patients have small lesions on nerve fibers, though DPN diagnosis has not been confirmed (Stino and Smith, 2017; Divisova et al., 2012) and there are currently no proven treatments for DPN (Azmi et al., 2021). Despite the complex pathogenesis of DPN, it has been documented that hyperglycemia plays a major role in the pathogenesis of DPN (Grisold et al., 2017; Pai et al., 2021). Thus, we explored the relationship between glucose concentration and SC viability. DMEM with 1 g/L or 4.5 g/L glucose is commonly used in media, and we found that SC viability in the low glucose group (1 g/L) was better than that in the normal glucose group (4.5 g/L) (Figure S1). The reason may be related to the fact that the glucose concentration of 4.5 g/L is higher than the normal blood glucose concentration *in vivo* when the carbon source is not depleted (Li et al., 2022). Besides, 1 g/L was also used in many SC studies as the control group (Yuan et al., 2022; Liu et al., 2021). Therefore, we think it is more reasonable to use 1 g/L as the control in the subsequent experiment. A high glucose concentration of more than 5.4 g/L is used in the literature. According to the reference (Wang et al., 2020b) and our experiment results (Figure S1), high glucose concentration and cell viability are negatively correlated and 18 g/L was used as the high glucose concentration. Furthermore, SC apoptosis was increased at high glucose concentrations and was positively correlated with the concentration (Liu et al., 2016). In conclusion, high glucose affects SC status and may mediate DPN.

Multiple miRNAs were down- and upregulated in diabetes, and have been shown not only to play an important role in the pathogenesis of T2D (Moura et al., 2014; Ozdemir and Feinberg, 2019) but also to be potential biomarkers for the development and progression of T2D as estimated by their circulating levels (Dehwah et al., 2012). Recent studies have reported that miR-21 is involved in regulating T2D glucose metabolism by promoting insulin secretion, further revealing the potential mechanism of miR-21 in regulating the pathogenesis of DPN (Liu et al., 2022a, 2022b). As a widely studied miRNA molecule, miR-21 was found to be closely related to peripheral neuropathy (Karl et al., 2022). Previous studies have focused on experiments *in vivo*, which have confirmed reduced levels of miR-21 in peripheral nerve and circulation in T2D model mice (Wang et al., 2020a; Wu et al., 2020), suggesting that miR-21 is involved in DPN. Here, we

demonstrated that miR-21 levels were also reduced in the peripheral nerve and circulation exosomes of T1D model rats, further suggesting exosomal miR-21 has a close relationship with DPN.

The AKT signaling pathway can be positively regulated by miR-21 (Deng et al., 2016), and is related to the proliferation and apoptosis of SC (Liu et al., 2020; Ma et al., 2021). It is also reported that miR-21 can protect neurons from cell apoptosis by targeting the AKT signaling pathway (Lv et al., 2020; Feng et al., 2018a). This suggests that the AKT signaling pathway may be involved in miR-21-mediated DPN. When SC were exposed to a high-glucose environment, the proliferation of SC was inhibited and cell apoptosis increased, and the expression of miR-21 and *p*-AKT in cells and exosomes was markedly decreased. By knocking down miR-21 for an in-depth study, SC viability was reduced and cell apoptosis was increased, thus further confirming the involvement of miR-21 in the effect of glucose on SC. Protective effects on SC exposed to high glucose were found when the expression of miR-21 was upregulated, and *p*-AKT expression increased. It has also been reported that upregulating the level of miR-21 inhibits neuronal apoptosis and improves proliferation activity (Zhan et al., 2022). In conclusion, changes in the expression of miR-21 *in vivo* and exosomes in SC under a high glucose environment play a profound role in regulating the occurrence and development of DPN.

Exosomes have therapeutic potential for the treatment of diabetes and diabetic complications (Hu et al., 2020). Exosomes, as extracellular vesicles, are rich in a variety of proteins and genetic material. Many studies have supported the roles of exosomes in intercellular communication through paracrine signaling in DPN (Singh et al., 2021; Fan et al., 2020). As essential components of exosomes, miRNAs have attracted much attention in exosomal function studies (Liu et al., 2022b; Fan et al., 2021). Additionally, *in vitro* data showed that SC-derived exosomes promoted neurite outgrowth of DPN. Above all, SC-derived exosomes modulation of miRNAs contributes to this therapy (Wang et al., 2020a, 2020b). It has been discovered that exosomes from SC that were exposed to high glucose conditions had high expression of miR-28, miR-31a, and miR-130a, and played a role in promoting the development of DPN (Jia et al., 2018). Healthy SC-derived exosomes were enriched with miR-21 and were effective for the treatment of DPN in T2D mice. In addition, exosomal miR-21 from adipose mesenchymal stem cells (MSCs) can also promote diabetic wound healing (Lv et al., 2020). Pathological processes of DPN include oxidative stress (Zhang et al., 2020b), inflammatory reaction (Feng et al., 2018b), and autophagy (Chung et al., 2018), which can be regulated by miR-21 (Yuan et al., 2020; Loboda et al., 2016; Zhang et al., 2020a), underscoring the importance of further exploring the role of miR-21 in DPN.

NG108-15 cells have been extensively used as neuronal cell lines in the literature (Ching et al., 2018; Kingham et al., 2007; Fu et al., 1997). When treated with SC-derived exosomes exposed to high glucose, NG108-15 cells' neurite outgrowth was inhibited and *p*-AKT expression was decreased compared with SC-derived exosomes exposed to low glucose. Finally, to further confirm the effect of exosomal miR-21 on neurite growth of neurons, we obtained exosomes with high expression of miR-21 by stably transfecting SC cell lines by using lentivirus, and observed that neurite outgrowth in NG108-15 cells was accelerated when treated with SC-derived exosomes rich in miR-21; moreover, *p*-AKT expression was also increased. Thus, SC-derived exosomal miR-21 participates in the high glucose regulation of NG108-15 cells neurite outgrowth. It has also been reported that the upregulation of exosomal miR-21 inhibits neuronal apoptosis by activating the AKT pathway (Sun et al., 2021; Cong et al., 2021), and increased the protein synthesis of axons, which has been shown to enhance the regeneration of injured axons. Moreover, the inhibition of exosomal miR-21 eliminated the protective effects of neurons via the AKT pathway (Gao et al., 2020). Our previous results also showed that SC-derived exosomal miR-21 promoted neurite outgrowth *in vitro* (Liu et al., 2022a, 2022b), while upregulation of miR-21 in MSCs-derived exosomes can also inhibit neuronal apoptosis (Xu et al., 2019). Together with results from *in vivo* studies (Wang et al., 2020a), we believe that SC-derived exosomal miR-21 is involved in the pathogenesis of DPN and may be a promising target for DPN treatment. The number of samples was determined by commonly used animal and cell experiments (Kwon et al., 2021). Ideally, the sample size should be calculated based on the t-test and F-test. In conclusion, a high-glucose environment mediated neuronal axon growth through exosomal miR-21 secreted by SC and may be an important mechanism for the development of DPN.

Neuronal damage occurs in the prediabetic stage (Celikbilek et al., 2014), and differentially expressed RNAs play critical roles in regulating the functions of SC involved in the pathogenesis of DPN (Wang et al., 2020a). AKT signaling pathway has been proven to be candidate genes for DPN (Guo et al., 2020). Our results demonstrated that the expression of miR-21 was decreased in serum exosomes and sciatic nerve of T1D DPN rats, and the

content of miR-21 in SC and SC-derived exosomes was decreased in a high-glucose environment, which was deleterious to SC and neurite growth. Conversely, increasing the expression of SC-derived exosomal miR-21 promoted neurite growth, with the AKT signaling pathway likely being the downstream pathway. SC-derived exosomal miR-21 participates in the high glucose regulation of NG108-15 cells' neurite outgrowth. Overall, our research provides valuable new insights into DPN treatment by targeting SC-derived exosomal miR-21.

Limitations of the study

1) AKT signaling pathway needs further study, 2) the use of primary cells to generate more convincing data, and 3) *in vivo* experiments of SC-derived exosomal miR-21 based on existing research results.

STAR★METHODS

Detailed methods are provided in the online version of this paper and include the following:

- KEY RESOURCES TABLE
- RESOURCE AVAILABILITY
  - Lead contact
  - Materials availability
  - Data and code availability
- EXPERIMENTAL MODEL AND SUBJECT DETAILS
  - Animals
- METHOD DETAILS
  - Isolation of exosomes from serum
  - Culture of SC and transfection
  - Cell counting Kit-8 (CCK-8)
  - Terminal dUTP nick-end labeling assay (TUNEL)
  - Isolation and characterization of exosomes derived from SC
  - Culture of NG108-15 cells and injection of SC exosomes
  - Quantitative Real-time PCR (qPCR)
  - Western blot
  - Immunocytochemistry and neurite outgrowth
- QUANTIFICATION AND STATISTICAL ANALYSIS

SUPPLEMENTAL INFORMATION

Supplemental information can be found online at https://doi.org/10.1016/j.isci.2022.105141.

ACKNOWLEDGMENTS

This work was supported by grants from the Natural Science Foundation of China (Nos. 81873357 and 81970991), the Shanghai Talent Development Funding Scheme (No. 2019090), the Natural Science Foundation of Shanghai (No. 21ZR1463100) and the Program of Shanghai Academic Research Leader (22XD1423400).

AUTHOR CONTRIBUTIONS

Hai-dong Guo and Shui-jin Shao designed the study, and Yu-pu Liu, Ming-yue Tian, and Yi-duo Yang performed most of the biological experiments; Han Li, Tian-tian Zhao, and Jing Zhu fed the animals and collected the samples; Yu-pu Liu and Guo-hong Cui wrote the manuscript; Ming-yue Tian, Fang-fang Mou, and Guo-hong Cui carried out the data analysis and revised the manuscript. All authors reviewed and approved the final manuscript.

DECLARATION OF INTERESTS

No potential conflicts of interest were disclosed by the authors.

Received: May 3, 2022
Revised: August 6, 2022
Accepted: September 9, 2022
Published: October 21, 2022

REFERENCES

Azmi, S., Alam, U., Burgess, J., and Malik, R.A. (2021). State-of-the-art pharmacotherapy for diabetic neuropathy. Expert Opin. Pharmacother. *22*, 55–68.

Bouçanova, F., and Chrast, R. (2020). Metabolic interaction between Schwann cells and axons under physiological and disease conditions. Front. Cell. Neurosci. *14*, 148.

Celikbilek, A., Tanik, N., Sabah, S., Borekci, E., Akyol, L., Ak, H., Adam, M., Suher, M., and Yilmaz, N. (2014). Elevated neurofilament light chain (nfl) mRNA levels in prediabetic peripheral neuropathy. Mol. Biol. Rep. *41*, 4017–4022.

Ching, R.C., Wiberg, M., and Kingham, P.J. (2018). Schwann cell-like differentiated adipose stem cells promote neurite outgrowth via secreted exosomes and RNA transfer. Stem Cell Res. Ther. *9*, 1–12.

Chung, Y.C., Lim, J.H., Oh, H.M., Kim, H.W., Kim, M.Y., Kim, E.N., Kim, Y., Chang, Y.S., Kim, H.W., and Park, C.W. (2018). Calcimimetic restores diabetic peripheral neuropathy by ameliorating apoptosis and improving autophagy. Cell Death Dis. *9*, 1–18.

Cong, M., Shen, M., Wu, X., Li, Y., Wang, L., He, Q., Shi, H., and Ding, F. (2021). Improvement of sensory neuron growth and survival via negatively regulating PTEN by miR-21-5p-contained small extracellular vesicles from skin precursor-derived Schwann cells. Stem Cell Res. Ther. *12*, 80.

Dehwah, M.A.S., Xu, A., and Huang, Q. (2012). MicroRNAs and type 2 diabetes/obesity. J. Genet. Genomics *39*, 11–18.

Deng, W., Wang, Y., Long, X., Zhao, R., Wang, Z., Liu, Z., Cao, S., and Shi, B. (2016). Mir-21 reduces hydrogen peroxide-induced apoptosis in c-kit+ cardiac stem cells in vitro through pten/pi3k/Akt signaling. Oxid. Med. Cell. Longev. *2016*, 5389181.

Divisova, S., Vlckova, E., Hnojcikova, M., Skorna, M., Nemec, M., Dubovy, P., Dusek, L., Jarkovsky, J., Belobradkova, J., and Bednarik, J. (2012). Prediabetes/early diabetes-associated neuropathy predominantly involves sensory small fibres. J. Peripher. Nerv. Syst. *17*, 341–350.

Fan, B., Chopp, M., Zhang, Z.G., and Liu, X.S. (2021). Treatment of diabetic peripheral neuropathy with engineered mesenchymal stromal cell-derived exosomes enriched with microRNA-146a provide amplified therapeutic efficacy. Exp. Neurol. *341*, 113694.

Fan, B., Li, C., Szalad, A., Wang, L., Pan, W., Zhang, R., Chopp, M., Zhang, Z.G., and Liu, X.S. (2020). Mesenchymal stromal cell-derived exosomes ameliorate peripheral neuropathy in a mouse model of diabetes. Diabetologia *63*, 431–443.

Feng, M., Liu, C., Chen, L.I., Feng, W., Liu, M., Hai, H., and Lu, J. (2018a). Mir-21 attenuates apoptosis-triggered by amyloid-β via modulating pdcd4/pi3k/Akt/gsk-3β pathway in sh-sy5y cells. Biomed. Pharmacother. *101*, 1003–1007.

Feng, Y., Chen, L., Luo, Q., Wu, M., Chen, Y., and Shi, X. (2018b). Involvement of microRNA-146a in diabetic peripheral neuropathy through the regulation of inflammation. Drug Des. Dev. Ther. *12*, 171.

Fu, A.K., Ip, F.C., Lai, K.O., Tsim, K.W., and Ip, N.Y. (1997). Muscle-derived neurotrophin-3 increases the aggregation of acetylcholine receptors in neuron–muscle co-cultures. Neuroreport *8*, 3895–3900.

Gao, X., Xiong, Y., Li, Q., Han, M., Shan, D., Yang, G., Zhang, S., Xin, D., Zhao, R., Wang, Z., et al. (2020). Extracellular vesicle-mediated transfer of miR-21-5p from mesenchymal stromal cells to neurons alleviates early brain injury to improve cognitive function via the PTEN/Akt pathway after subarachnoid hemorrhage. Cell Death Dis. *11*, 363.

Grisold, A., Callaghan, B.C., and Feldman, E.L. (2017). Mediators of diabetic neuropathy-is hyperglycemia the only culprit? Curr. Opin. Endocrinol. Diabetes Obes. *24*, 103.

Guo, K., Eid, S.A., Elzinga, S.E., Pacut, C., and Hur, J. (2020). Genome-wide profiling of DNA methylation and gene expression identifies candidate genes for human diabetic neuropathy. Clin. Epigenetics *12*, 1–16.

Hicks, C.W., and Selvin, E. (2019). Epidemiology of peripheral neuropathy and lower extremity disease in diabetes. Curr. Diabetes Rep. *19*, 1–8.

Hu, W., Song, X., Yu, H., Sun, J., and Zhao, Y. (2020). Therapeutic potentials of extracellular vesicles for the treatment of diabetes and diabetic complications. Int. J. Mol. Sci. *21*, 5163.

Jagadeeswaran, G., Nimmakayala, P., Zheng, Y., Gowdu, K., Reddy, U.K., and Sunkar, R. (2012). Characterization of the small RNA component of leaves and fruits from four different cucurbit species. BMC Genom. *13*, 1–13.

Jia, L., Chopp, M., Wang, L., Lu, X., Szalad, A., and Zhang, Z.G. (2018). Exosomes derived from high-glucose-stimulated Schwann cells promote development of diabetic peripheral neuropathy. FASEB J. *32*, 6911–6922.

Kalluri, R., and LeBleu, V.S. (2020). The biology, function, and biomedical applications of exosomes. Science *367*, u6977.

Karl, F., Grießhammer, A., Üçeyler, N., and Sommer, C. (2017). Differential impact of mir-21 on pain and associated affective and cognitive behavior after spared nerve injury in b7-h1 ko mouse. Front. Mol. Neurosci. *10*, 219.

Karl, F., Kunz, M., Kress, L., Held, M., Egenolf, N., Wiesner, A., Dandekar, T., Sommer, C., and Uceyler, N. (2022). A translational study: involvement of miR-21-5p in development and maintenance of neuropathic pain via immune-related targets CCL5 and YWHAE. Exp. Neurol. *347*, 113915.

Kingham, P.J., Kalbermatten, D.F., Mahay, D., Armstrong, S.J., Wiberg, M., and Terenghi, G. (2007). Adipose-derived stem cells differentiate into a Schwann cell phenotype and promote neurite outgrowth in vitro. Exp. Neurol. *207*, 267–274.

Kwon, J., Arsenis, C., Suessmilch, M., McColl, A., Cavanagh, J., and Morris, B.J. (2021). Differential effects of toll-like receptor activation and differential mediation by map kinases of immune responses in microglial cells. Cell. Mol. Neurobiol. 1–17.

Levitt, N.S., Stansberry, K.B., Wynchank, S., and Vinik, A.I. (1996). The natural progression of autonomic neuropathy and autonomic function tests in a cohort of people with iddm. Diabetes Care *19*, 751–754.

Li, Z., Nees, M., Bettenbrock, K., and Rinas, U. (2022). Is energy excess the initial trigger of carbon overflow metabolism? Transcriptional network response of carbon-limited Escherichia coli to transient carbon excess. Microb. Cell Fact. *21*, 67.

Liu, D., Liang, X., and Zhang, H. (2016). Effects of high glucose on cell viability and differentiation in primary cultured schwann cells: potential role of ERK signaling pathway. Neurochem. Res. *41*, 1281–1290.

Liu, J.Y., Zhang, Y.C., Xie, R.R., Song, L.N., Yang, W.L., Xin, Z., Cao, X., and Yang, J.K. (2021). Nifuroxazide improves insulin secretion and attenuates high glucose-induced inflammation and apoptosis in INS-1 cells. Eur. J. Pharmacol. *899*, 174042.

Liu, R., Liu, C., He, X., Sun, P., Zhang, B., Yang, H., Shi, W., and Ruan, Q. (2022a). MicroRNA-21 promotes pancreatic beta cell function through modulating glucose uptake. Nat. Commun. *13*, 3545.

Liu, Y.P., Yang, Y.D., Mou, F.F., Zhu, J., Li, H., Zhao, T.T., Zhao, Y., Shao, S.J., Cui, G.H., and Guo, H.D. (2022b). Exosome-mediated miR-21 was involved in the promotion of structural and functional recovery effect produced by electroacupuncture in sciatic nerve injury. Oxid. Med. Cell. Longev. *2022*, 7530102.

Liu, Y., Shao, S., and Guo, H. (2020). Schwann cells apoptosis is induced by high glucose in diabetic peripheral neuropathy. Life Sci. *248*, 117459.

Loboda, A., Sobczak, M., Jozkowicz, A., and Dulak, J. (2016). Tgf-β1/smads and mir-21 in renal fibrosis and inflammation. Mediat. Inflamm. *2016*, 1–12.

Lopez Verrilli, M.A., Picou, F., and Court, F.A. (2013). Schwann cell-derived exosomes enhance axonal regeneration in the peripheral nervous system. Glia *61*, 1795–1806.

Luo, J., Ning, X., Wang, H., Liang, J., and Lu, X. (2017). MicroRNA-21 promotes axonal regeneration of peripheral nerve cells through regulating epha4 expression in Schwann cells. Int. J. Clin. Exp. Med. *10*, 14203–14212.

Lv, X., Liang, J., and Wang, Z. (2020). Mir-21-5p reduces apoptosis and inflammation in rats with spinal cord injury through pi3k/Akt pathway. Panminerva Med. https://doi.org/10.23736/S0031-0808.20.03974-9.

Ma, Y., Zhou, D., Zhang, H., Tang, L., Qian, F., and Su, J. (2021). Human Umbilical cord mesenchymal stem cell-derived extracellular vesicles promote the proliferation of schwann cells by regulating the PI3K/AKT signaling pathway via transferring miR-21. Stem Cells Int. *2021*, 1496101.

Moura, J., Børsheim, E., and Carvalho, E. (2014). The role of microRNAs in diabetic complications—special emphasis on wound healing. Genes-Basel *5*, 926–956.

Ning, X., Lu, X., Luo, J., Chen, C., Gao, Q., Li, Z., and Wang, H. (2020). Molecular mechanism of microRNA-21 promoting Schwann cell proliferation and axon regeneration during injured nerve repair. RNA Biol. *17*, 1508–1519.

O'Brien, J., Hayder, H., Zayed, Y., and Peng, C. (2018). Overview of microRNA biogenesis, mechanisms of actions, and circulation. Front. Endocrinol. *9*, 402.

Ozdemir, D., and Feinberg, M.W. (2019). MicroRNAs in diabetic wound healing: pathophysiology and therapeutic opportunities. Trends Cardiovas Med. *29*, 131–137.

Pai, Y., Tang, C., Lin, C., Lin, S., Lee, I., and Chang, M. (2021). Glycaemic control for painful diabetic peripheral neuropathy is more than fasting plasma glucose and glycated haemoglobin. Diabetes Metab. *47*, 101158.

Sakai, A., and Suzuki, H. (2013). Nerve injury-induced upregulation of mir-21 in the primary sensory neurons contributes to neuropathic pain in rats. Biochem Bioph. Res. Co. *435*, 176–181.

Salzer, J.L. (2015). Schwann cell myelination. Csh Perspect Biol. *7*, a20529.

Singh, A., Raghav, A., Shiekh, P.A., and Kumar, A. (2021). Transplantation of engineered exosomes derived from bone marrow mesenchymal stromal cells ameliorate diabetic peripheral neuropathy under electrical stimulation. Bioact. Mater. *6*, 2231–2249.

Stino, A.M., and Smith, A.G. (2017). Peripheral neuropathy in prediabetes and the metabolic syndrome. J. Diabetes Invest. *8*, 646–655.

Sullivan, T.B., Robert, L.C., Teebagy, P.A., Morgan, S.E., Beatty, E.W., Cicuto, B.J., Nowd, P.K., Rieger-Christ, K.M., and Bryan, D.J. (2018). Spatiotemporal microrna profile in peripheral nerve regeneration: mir-138 targets vimentin and inhibits schwann cell migration and proliferation. Neural. Regen. Res. *13*, 1253.

Sun, T., Duan, L., Li, J., Guo, H., and Xiong, M. (2021). Gypenoside XVII protects against spinal cord injury in mice by regulating the microRNA21mediated PTEN/AKT/mTOR pathway. Int. J. Mol. Med. *48*, 146.

Wang, L., Chopp, M., Szalad, A., Lu, X., Zhang, Y., Wang, X., Cepparulo, P., Lu, M., Li, C., and Zhang, Z.G. (2020a). Exosomes derived from Schwann cells ameliorate peripheral neuropathy in type 2 diabetic mice. Diabetes *69*, 749–759.

Wang, X., Yi, H., Li, C., Cao, H., and Shen, Z. (2020b). Diphenyl diselenide alleviates diabetic peripheral neuropathy in rats with streptozotocin-induced diabetes by modulating oxidative stress. Biochem. Pharmacol. *182*, 114221.

Wu, Y., Zhang, K., Liu, R., Zhang, H., Chen, D., Yu, S., Chen, W., Wan, S., Zhang, Y., and Jia, Z. (2020). Microrna-21-3p accelerates diabetic wound healing in mice by downregulating spry1. Aging (Albany NY) *12*, 15436.

Xu, G., Ao, R., Zhi, Z., Jia, J., and Yu, B. (2019). miR-21 and miR-19b delivered by hMSC-derived EVs regulate the apoptosis and differentiation of neurons in patients with spinal cord injury. J. Cell. Physiol. *234*, 10205–10217.

Yu, B., Zhou, S., Qian, T., Wang, Y., Ding, F., and Gu, X. (2011). Altered microrna expression following sciatic nerve resection in dorsal root ganglia of rats. Acta Biochim. Biophys. Sin. *43*, 909–915.

Yu, X., Odenthal, M., and Fries, J.W. (2016). Exosomes as mirna carriers: formation–function–future. Int. J. Mol. Sci. *17*, 2028.

Yuan, M., Yang, X., Duscher, D., Xiong, H., Ren, S., Xu, X., Wang, C., Chen, J., Liu, Y., and Machens, H. (2020). Overexpression of microrna-21-5p prevents the oxidative stress-induced apoptosis of rsc96 cells by suppressing autophagy. Life Sci. *256*, 118022.

Yuan, Q., Zhang, X., Wei, W., Zhao, J., Wu, Y., Zhao, S., Zhu, L., Wang, P., and Hao, J. (2022). Lycorine improves peripheral nerve function by promoting Schwann cell autophagy via AMPK pathway activation and MMP9 downregulation in diabetic peripheral neuropathy. Pharmacol. Res. *175*, 105985.

Zhan, L., Pang, Y., Jiang, H., Zhang, S., Jin, H., Chen, J., Jia, C., Guo, H., and Mu, Z. (2022). Butylphthalide inhibits TLR4/NF-kappaB pathway by upregulation of miR-21 to have the neuroprotective effect. J. Healthc Eng. *2022*, 4687349.

Zhang, H.H., Huang, Z.X., Zhong, S.Q., Fei, K.L., and Cao, Y.H. (2020a). Mir-21 inhibits autophagy and promotes malignant development in the bladder cancer t24 cell line. Int. J. Oncol. *56*, 986–998.

Zhang, Y., Zhou, Z., Song, C., and Chen, X. (2020b). The protective effect and mechanism of dexmedetomidine on diabetic peripheral neuropathy in rats. Front. Pharmacol. *11*, 1139.

Zhou, S., Zhang, S., Wang, Y., Yi, S., Zhao, L., Tang, X., Yu, B., Gu, X., and Ding, F. (2015). Mir-21 and mir-222 inhibit apoptosis of adult dorsal root ganglion ganglion neurons by repressing TIMP3 following sciatic nerve injury. Neurosci. Lett. *586*, 43–49.

STAR★METHODS

KEY RESOURCES TABLE

REAGENT or RESOURCE	SOURCE	IDENTIFIER
Antibodies		
Rabbit anti-NF200	Sigma-Aldrich	Cat# N4142; RRID:AB_477272
Rabbit anti-MBP	Abcam	Cat# ab40390; RRID:AB_1141521
Rabbit anti-CD9	Abcam	Cat# ab92726; RRID:AB_10561589
Rabbit anti-CD63	Abcam	Cat# ab108950; RRID:AB_10863101
Rabbit anti-p-AKT	CST	Cat# 4060; RRID:AB_2315049
Rabbit anti-t-AKT	CST	Cat# 4691; RRID:AB_915783
Rabbit anti-Bcl-2	Abcam	Cat# ab59348; RRID:AB_2064155
Rabbit anti-Bax	CST	Cat# 2772; RRID:AB_10695870
Rabbit anti-Cleaved Caspase-3	CST	Cat# 9664; RRID:AB_2070042
Rabbit anti-DNMT3A	Abcam	Cat# ab2850; RRID:AB_303355
Rabbit anti-GAP43	Abcam	Cat# ab12274; RRID:AB_2247459
Mouse anti-GAPDH	Proteintech	Cat# CL594-60004; RRID:AB_2919886
Rabbit anti-beta III Tubulin	Abcam	Cat# ab18207; RRID:AB_444319
Goat anti-rabbit Alexa Fluor 555	Invitrogen	Cat# A27039; RRID:AB_2536100
Anti-rabbit HRP	CST	Cat# 7074; RRID:AB_2099233
Anti-mouse HRP	CST	Cat# 7076; RRID:AB_330924
Anti-rabbit Alexa Fluor 555	Invitrogen	Cat# A-21428; RRID:AB_2535849
Chemicals, peptides, and recombinant proteins		
miR-21-5p mimic	Ribobio	miR10000790-1-5
miR-21-5p inhibitor	Ribobio	miR20004711-1-5
TRIzol	Life technologies	A33251
miRcute Plus miRNA First-Strand cDNA Synthesis Kit	Tiangen	KR211-02
FastKing gDNA Dispelling RT SuperMix Kit	Tiangen	KR118-02
Lipofectamine 3000	Invitrogen	L3000015
Lipofectamine 2000	Invitrogen	11668-019
CCK-8	Kumamoto	CK04-11
FBS	C0235	Invitrogen
DMEM	Corning Cellgro™	10-013-CV
TUNEL reaction buffer	Invitrogen	C10246
Hoechst 33342	Invitrogen	62249
ECL	Millipore	WBKLS0100
Bradford protein assay	5000204	BioRad
Streptozotocin	Sigma-Aldrich	20130
PFA	Sigma-Aldrich	158127
Experimental models: Cell lines		
NG108-15	ATCC	HB-12317
RSC96	ATCC	CRL-2765

RESOURCE AVAILABILITY

Lead contact

Further information and requests for resources and reagents should be directed to and will be fulfilled by the lead contact, Shui-jin Shao (shaoshuijin@163.com).

Materials availability

This study did not generate new unique reagents and all materials mentioned in the manuscript are available from the lead contact on request.

Data and code availability

Data reported in this paper will be shared by the lead contact upon request. This paper does not report novel gene/RNA sequences and original code. Any additional information from the data reported in this paper is available from the lead contact on request.

EXPERIMENTAL MODEL AND SUBJECT DETAILS

Animals

Ethics approval: All experimental procedures involved in this study were authorized by the animal ethics committee of Shanghai University of TCM and the Animal Research Committee of Shanghai (ethics number: PZSHUTCM200628003). The animal experiments were complied with the ARRIVE guidelines as well as the National Institute of Health's Guide for the Care and Use of Laboratory Animals, And efforts were made to reduce the number of rats and improve the utilization rate of rats as far as possible during the whole procedure.

Establishment of the T1D DPN model: 20 male SD rats weighing between 180 and 190g (7-week-old) were purchased from the Animal Experimental Center of Shanghai University of Traditional Chinese Medicine (license number: SYXK2020-0009). After one week of adaptive feeding, rats were randomly divided into 2 groups. Streptozotocin (STZ; 20,130 Sigma-Aldrich) was administrated to induce T1D DPN by an intraperitoneal injection of 50 mg/kg (DPN group), and the control group was treated with 0.1 M citrate buffer with PH-4.5. Blood glucose levels were estimated after 48 h, and rats with glucose levels of more than 16.7 mM was supposed to have diabetics. Blood glucose levels were measured at 0, 1, 4, and 8 weeks to ensure that blood glucose levels were higher than 16.7 mM.

At the end of the eighth week, nerve conduction velocity (NCV) of the sciatic nerve was measured by an operator blinded to the treatment. The RM6240 Biological Signal Collecting System (Chengdu Instrument Factory, Chengdu, China) was used to record compound motor action potentials (CMAPs). After the rat was anesthetized with pentobarbital sodium, the stimulating electrodes were inserted proximal and distal to the injury site, respectively. The recording electrode was inserted into the gastrocnemius muscle with 5–10 V intensity of electrical stimulation and 0.2 ms of wavelength. NCV was calculated by dividing the distance between two stimulating points by the latency difference between two points.

After the measurement, the rats were sacrificed, and the sciatic nerve was extracted for immunofluorescence staining on transverse frozen sections. Neurofilament heavy chain (NF200; rabbit polyclonal 1:80; Sigma-Aldrich N4142) and myelin basic protein (MBP; rabbit polyclonal 1:100; Abcam ab40390) were used to stain axons and myelin, and goat anti-rabbit Alexa Fluor 555 (1:1,000; A-21428 Invitrogen) was used as the secondary antibody.

METHOD DETAILS

Isolation of exosomes from serum

The serum of rats was extracted by blood collection from the abdominal aorta and was subjected to centrifugation (10,000 g for 30 min at 4°C) at once, followed by ultracentrifugation at 100,000 g for 70 min (CS120FNX Hitachi; Japan). 0.1M cold PBS (PBS; PH 7.4) was used to wash the precipitation containing the exosomes, and the solution was centrifuged again at 100,000 g for 70 min; the exosomes were then re-suspended in PBS.

Culture of SC and transfection

RSC96 (rat SC line; CRL-2765 ATCC) cells were cultured in Dulbecco's Modified Eagle Medium (DMEM; 10-013-CV Corning Cellgro) containing low glucose (1 g/L), normal glucose (4.5 g/L) or high glucose (18 g/L) with 10% fetal bovine serum (FBS; C0235 Invitrogen). The incubator environment was 37°C, with 5% CO_2.

SC cultured in high glucose within 24 h were transfected with miR-21 control (MC) or miR-21-5p mimic (miR-21) (miR10000790-1-5 Ribobio; Guangzhou; China) combined with Lipofectamine 3000 reagent (L3000015

Invitrogen) according to the manufacturer's instructions. SC cultured in low glucose within 24 h were transfected with miR-21 control (NC) or miR-21-5p inhibitor (miR-21) (miR20004711-1-5 Ribobio; Guangzhou; China) combined with Lipofectamine 2000 reagent (11,668-019 Invitrogen) according to the manufacturer's instructions.

Cell counting Kit-8 (CCK-8)

RSC96 cells were plated on poly-L-lysine-coated 96-well plates (353072 Corning Falcon) at a density of 1×10^4 cells/ml. 72 h after different glucose concentration treatments or transfection under high glucose, 10 μL of CCK-8 (CK04-11 Dojido; Kumamoto; Japan) was added to each well, and the cells were incubated for 1 h at 37°C. The absorbance was read at 450 nm using a microplate reader (Synergy 2; BioTek; USA).

Terminal dUTP nick-end labeling assay (TUNEL)

At 72 h after treatment with different concentrations of glucose or transfection under high glucose, SC were fixed for 0.5 h on ice and then washed in PBS. For the TUNEL assay, the cells were incubated with 50 μL TUNEL reaction buffer (C10246 Invitrogen) for 1 h at 37°C in the dark. Nuclei were counterstained with Hoechst 33,342 (62,249 Invitrogen). The percentage of apoptotic SC were determined by counting the number of TUNEL-positive cells/total number of cells.

Isolation and characterization of exosomes derived from SC

Two methods were used to cultivate SC separately: 1) SC were cultured in DMEM with 10% exosome-free FBS (obtained by ultracentrifugation at 100,000 g for 20 h) containing low glucose (1 g/L) or high glucose (18 g/L). 2) Construction of 2 stably transfected SC cell lines, transfected using lentiviral vectors expressing an empty vector or a precursor of miR-21-5p respectively; SC were then cultured in DMEM with 10% exosome-free FBS.

After 72 h, the supernatant was subjected to a series of centrifugations (300 x g for 10 min, 2000 g for 10 min, 10,000 g for 30 min at 4°C), followed by ultracentrifugation at 100,000 g for 70 min (Hitachi; Japan). Cold 0.1M PBS (PH 7.4) was used to wash the precipitate containing the exosomes, and the solution was centrifuged again at 100,000 g for 70 min; the exosomes were then resuspended in PBS. The Bradford protein assay (5,000,204 BioRad) was used to measure the concentration of total protein in the exosomes (method 1: L-EXO and H-EXO; method 2: MC-EXO and miR-21-EXO).

Exosome markers (CD9, CD63; Abcam; UK) were detected by Western blot. The exosomal lysate was mixed with loading buffer, subjected to 10% SDS-PAGE electrophoresis, and then transferred to polyvinylidene fluoride (PVDF) membranes (FFP28 Millipore, USA). The following primary antibodies were used: anti-CD9 (rabbit monoclonal 1:2000; Abcam ab92726), anti-CD63 (mouse monoclonal 1:1000; Abcam ab108950), Secondary antibodies used were anti-rabbit HRP (1:8000; CST 7074) and anti-mouse HRP (1:8000; CST 7076). Protein expression levels were visualized by enhanced chemiluminescence (ECL; WBKLS0100 Millipore).

Culture of NG108-15 cells and injection of SC exosomes

NG108-15 cells (HB-12317 ATCC) were cultured in DMEM with 10% FBS and supplemented with 0.1 mM hypoxanthines, 400 nM aminopterin, and 16 μM thymidine (H9377, A1784, and T1895 Sigma-Aldrich). NG108-15 cells were plated on a 60 mm cell culture dish or a 35 mm confocal dish in DMEM and cultured in 10% exosome-free FBS. After plating, 4 types of SC exosomes (L-EXO and H-EXO; MC-EXO and miR-21-EXO; 15/5 μg resuspended in PBS) were added daily for 3 days.

Quantitative Real-time PCR (qPCR)

SC and NG108-15 cells were trypsinized and collected by centrifugation, and the total RNA of cells and sciatic nerve was extracted from the cells by TRIzol (A33251 Life technologies; Carlsbad; CA). The miRNeasy Serum/Plasma Advanced Kit (Qiagen 217,184) was used to isolate the miRNAs from SC exosomes and serum exosomes. miRcute Plus miRNA First-Strand cDNA Synthesis Kit and FastKing gDNA Dispelling RT Super-Mix Kit (KR211-02 and KR118-02 Tiangen, Beijing, China) was used to reverse-transcribe total RNA and miRNAs and for amplification.

Rat primer of miR-21-5p: 5′-GTAGCTTATCAGACTGATGTTGA-3′; U6: 5′-CTCGCTTCGGCAGCACA-3′; v-akt murine thymoma viral oncogene homolog 1 (AKT1): 5′-CTCATTCCAGACCCACGAC-3′, 5′-ACAGCCC GAAGTCCGTTA-3′; DNA methyltransferase 3A (DNMT3A): 5′-CAGCAAAGTGAGGACCATTA-3′, 5′-AA CACCCTTTCCATTTCAG-3′; Growth Associated Protein 43 (GAP43): 5′-GAGGGAGATGGCTCTGCTACT-3′, 5′-GCTTCATCTACAGCTTCTTTC-3′; Glyceraldehyde-3-Phosphate Dehydrogenase (GAPDH): 5′-ATGACTC TACCCACGGCAAG-3′, 5′-GGAAGATGGTGATGGGTTTC-3′.

Western blot

RIPA and protease inhibitors (ThermoFisher Scientific) were used to extract protein lysates from SC and NG108-15 cells, and a BCA protein assay kit (23,225 Pierce; Rockford; IL) was used to measure the protein concentration. The steps were as described above. The membranes were incubated with primary antibodies at 4°C over-night after blocked with 5% skim milk at room temperature for 1 h. The following primary antibodies used were: anti-*p*-AKT (rabbit polyclonal 1:2000; CST 4060), anti-*t*-AKT (rabbit polyclonal 1:1000; CST 4691), anti-Bcl-2 (rabbit monoclonal 1:1000; Abcam ab59348), anti-Bax (rabbit polyclonal 1:1000; CST 2772), anti-Cleaved Caspase-3 (C-cas3)(rabbit polyclonal 1:1000; CST 9664), anti-DNMT3A (rabbit monoclonal 1:500; Abcam ab2850), anti-GAP43 (rabbit monoclonal 1:1000; Abcam ab12274), anti-GAPDH (mouse monoclonal 1:20,000; Proteintech 60,004). After addition of the anti-rabbit or anti-mouse secondary antibody at room temperature for 2 h, the protein bands on the membranes were detected using an enhanced chemilumines-cence system and a Bio-Spectrum Gel Imaging System, respectively. The gray value statistics was analyzed by ImageJ.

Immunocytochemistry and neurite outgrowth

After treatment with SC exosomes for 3 days, NG108-15 cells cultured in a 35 mm confocal dish were fixed with ice-cold 4% paraformaldehyde (PFA; 158,127 Sigma-Aldrich) for 20 min, permeabilized with 0.5% Triton X-100 (X100 Sigma-Aldrich) for 15 min and blocked with 10% goat serum (G9023 Sigma-Aldrich) for 1 h. Anti-beta III Tubulin (βIII) (rabbit monoclonal 1:2000; Abcam **ab18207)** was used as the primary antibody over-night at 4°C, and goat anti-rabbit Alexa Fluor 555 (1:1,000; Invitrogen A27039) was used as the secondary antibody 2 h at room temperature. Hoechst 33,342 was used to stain the nuclei. After washing with PBS, fluorescently labeled NG108-15 cell bodies and neurites were imaged using an inverted fluores-cence microscope (IX53, Olympus, Japan). Neurite length in the images was measured using the ImageJ program.

QUANTIFICATION AND STATISTICAL ANALYSIS

Parametric test data presented as bar graphs (blue) were mean values ±SD. SPSS 22.0 was used to detect the normality and uniform variance of the sample (satisfy normality and uniform variance when $p > 0.05$). Statistical analysis was performed using one-way ANOVA followed by Scheffe's post hoc multiple-comparison for 3-group or a Student's *t* test was used for 2-groups when the sample satisfy normality and uniform variance (Lg-transformation was conducted to normalize the distribution of the sample which didn't satisfy normality and uniform variance). Nonparametric tests were used when the samples were few, had high variability, or did not satisfy uniform variance. Nonparametric test data were presented as bar graphs (red) are the median and interquartile range. Differences with $p < 0.05$ were considered statistically significant.